Bulletin of the Seismological Society of America, Vol. 88, No. 2, pp. 621–632, April 1998

On the Mechanism of Conversion of Seismic Waves to and from *T* Waves in the Vicinity of Island Shores

by Jacques Talandier and Emile A. Okal

Abstract High-frequency seismic records from the Polynesian Seismic Network are used to investigate in detail the processes of conversion of acoustic (*T*-wave) energy from and to seismic waves at island shores. On the source side, we study the seismic-to-acoustic conversion based on *T* phases from Hawaiian events recorded at Polynesian stations located on the coral platter; on the receiver side, we study the acoustic-to-seismic conversion based on *T* phases from marine sources recorded across the Polynesian islands. In both instances, our results underline the importance of steep slopes (typically 50°) in allowing an efficient conversion between *P* waves in the island structure and *T* waves in the water column. These slopes can be coral reefs or the heads of young, presumably unconsolidated, basalt flows. Under this geometry, modeling based on raytracing indicates that the seismic record of the *T* phase consists of a *P* wave at distances from the conversion point greater than 9 km; at shorter distances, *S* waves and surface waves are generated. In the absence of a steep slope, only surface waves are present. These models can be used to compute precise and predictable travel-time station corrections, allowing the use of seismometers located inland to exploit the superb detection and location capabilities of *T* waves.

Introduction

The purpose of this article is to investigate the processes of conversion of seismic waves to and from acoustic energy, which can result in the efficient excitation of *T* waves by seismic sources located inland and, following their propagation in the SOFAR channel, in their possible recording by seismometers deployed on land, occasionally at distances of several tens of kilometers from the closest shore.

Even though *T* waves are elastic modes of the ocean water column channeled through the low-velocity SOFAR wave guide and, as such, should be recorded only at sea on hydrophones, they are routinely detected by land-based seismometers; indeed, it is interesting to note that *T* waves were first identified (Anonymous, 1930) and correctly interpreted (Linehan, 1940; Ravet, 1940) from seismic records. This, and the fact that wavetrains of *T* phases have occasionally been felt by island populations (Talandier and Okal, 1979), indicates that an efficient conversion of acoustic waves to seismic energy can take place at seashores, at least under favorable conditions. The converse is obviously of significant interest, since it allows the excitation of *T* phases by earthquakes whose hypocenter is *a priori* outside the oceanic column and can be of intermediate depth, or even deep (Talandier and Okal, 1979; Okal and Talandier, 1997).

Together with the channeling efficiency of the SOFAR wave guide, the all but negligible anelastic attenuation in the water column makes for an exceptionally efficient transmission of *T*-wave energy at teleseismic distances and thus results in superb detection capabilities. Also, their relatively slow speed (1484 m/sec across most of the Pacific Ocean) results in excellent precision for locations based on *T*-wave times; this combined performance in detection and location makes *T* waves a choice tool for the monitoring and identification of small sources in remote areas, and thus the Comprehensive Test Ban Treaty has mandated an acoustic network as part of the International Monitoring System.

In this general framework, it is important to obtain a more profound understanding of the mechanisms involved in the conversion of seismic energy to acoustic (*T*) energy at a shoreline close to the seismic source and, conversely, in the generation of seismic energy when the *T* wave hits a continental shelf or island shore. These two processes are investigated separately in the present article. In the second section, we analyze the source-side (seismic-to-acoustic) process by studying *T*-phase records of Hawaiian events at Polynesian seismic stations, while in the third section, we use marine sources in and outside Polynesia to investigate the receiver-side (acoustic-to-seismic) conversion and the propagation of the resulting seismic phases through the islands of French Polynesia. Early results using a similar approach, albeit only on the receiver side, were obtained on

the Island of Hawaii by Koyanagi *et al.* (1995). Note, however, that these authors used records across the island of *T* waves from earthquakes themselves located inland (35 km in the case of the Loma Prieta event), which makes it difficult to separate the two conversion processes. More recently, McLaughlin (1997) has discussed the reception of *T* waves at an island station off the coast of southern California. In the case of a continental shelf, Cansi and Bethoux (1985) also modeled the propagation of converted *T* waves across Europe as L_g and R_g phases. On the theoretical side, Piserchia *et al.* (1997) have used finite-difference techniques to model the interaction of an incoming *T* wave (computed far from the coastline using a Maslov ray approach) with an island structure.

In all instances, we use records from the French Polynesian Seismic Network (Réseau Sismique Polynésien, hereafter RSP), which has been described in a number of previous publications to which the reader is referred (Talandier and Kuster, 1976; Okal *et al.*, 1980; Talandier, 1993) and whose general layout is shown in Figure 1. We simply underscore here several characteristics of the RSP: First, the regular short-period channels use a combination of filters (band rejection peaked at 0.33 Hz, and high-pass cornered at 0.30 Hz), which eliminates background noise related to sea swell, resulting in routine magnifications at oceanic sites comparable to continental standards (125,000 at 1 Hz). In addition, a special "*T*-wave channel" band-passed between 2 and 10 Hz features magnifications of 2×10^6 at 3 Hz, thus allowing exceptional detection capabilities. Broadband records are also available in digital form. Finally, several atoll stations are deployed less than 100 m from the near-vertical outboard underwater cliff of the coral reef [e.g., Pomariorio (PMO) in the North and Vaihoa (VAH) in the South of Rangiroa Atoll; see Fig. 1]. In the appropriate geometry, the onland propagation becomes negligible, and the relevant record can be taken as representative of the acoustic *T* phase as it exists in the ocean. For example, by using PMO records from Hawaiian events, we suppress any receiver contribution to the seismogram and isolate the source-side, seismic-to-acoustic process, as we now describe in the next section.

Mechanism of the Seismic-to-Acoustic Conversion

The dataset used in this section consists of records obtained at PMO from the earthquake of 8 June 1993 (m_b = 5.2) on the southern flank of the Island of Hawaii (hereafter the "Big" Island) and from the strongest event (29 July 1996; m_b = 4.4) of the volcanic swarm at Loihi Seamount (≈45 km south of the Big Island) during the summer of 1996. In the next paragraphs, we illustrate our methodology in detail on the first event and give more succinct results for the second event. Similar results were also obtained for the two recent earthquakes of 16 March 1997 (m_b = 4.2) and 30 June 1997 (m_b = 5.3).

The Hawaii Earthquake of 8 June 1993

We use the hypocentral location and origin time as determined by the NEIC based on 160 arrival times, including about 50 from the Hawaiian Volcano Observatory (HVO) network: 19.328° N; 155.220° W; depth, 4 km; origin time, 12:57:49.4 GMT. This places the event south of the Chain of Craters Road, in the vicinity of the Poliokeawe Pali. Figure 2 shows the short-period vertical record of the *T* phase at PMO. In the relevant range of frequencies, the instrument response is flat to velocity, and the seismogram can be read directly as ground velocity. The following observations are immediate: The record consists of two main arrivals separated by approximately 2.4 sec; the arrivals are impulsive, suggesting that the seismic-to-acoustic conversion is a relatively simple process; and the peak-to-peak amplitude (15 μm/sec) is large, indicating that the conversion process is efficient. Finally, we note that the spectral content of the two

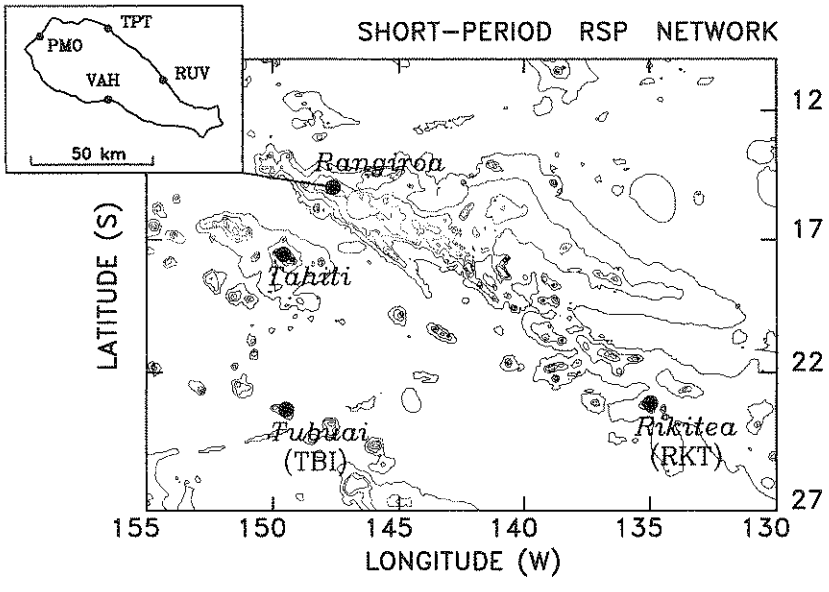

Figure 1. Map of the French Polynesian Seismic Network. The insert at upper left shows the subarray on Rangiroa Atoll. The Society Islands subarray is detailed in Figure 10. Interval between isobaths is 1000 m.

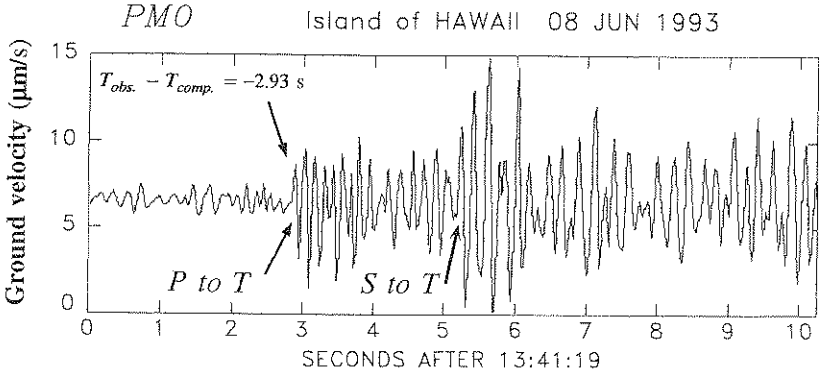

Figure 2. *T*-wave seismogram at Pomariorio (PMO) from the Hawaiian earthquake of 8 June 1993.

arrivals appears different, even in this time-domain plot. This and the delay between the two arrivals suggest that the first one represents a *T* wave generated by conversion of the near-field *P* wave, whereas the second arrival corresponds to an *S*-to-*T* conversion.

Methodology. Because the path from hypocenter to receiving shore will comprise a land component close to the source, traveled at seismic velocity, as well as an oceanic fraction, the arrival time of the *T* phase will be different from that expected, had the whole path been oceanic. We thus define the residual

$$\text{Res} = t_{\text{Obs}} - t_{\text{Refer}} \qquad (1)$$

as the difference between the arrival time of the *T* phase observed on the record and the reference time predicted for a purely oceanic propagation from the epicenter to the receiving shore, the latter being computed using a regionalized 1° grid of *T*-wave velocities (Levitus *et al.*, 1994). In the present example, for the first arrival, Res = −2.93 sec is negative, indicating simply that the land portion travels faster than would an oceanic wave, and thus the *T* wave at PMO is slightly early.

We seek to model the residual, Res, by studying the travel time of a seismic wave (which could be *a priori P* or *S*) between the hypocenter and a conversion point favorable for the generation of a *T* wave into the SOFAR channel. The geometry of this conversion is obviously controlled by the three-dimensional bathymetry of the ocean floor in the vicinity of the epicenter, on a scale comparable to the wavelength of the relevant *T* waves that is, a few hundred meters. We use for this purpose the fine-scale bathymetry of the southern shore of the Island of Hawaii, recently compiled by Smith (1994) and degraded to a gridding of 3 sec of arc in both latitude and longitude.

We present in Figure 3 a cross section of the island and the neighboring seafloor in the immediate vicinity of the plane of the great circle, where a small segment of seafloor features a steep (50°) slope, immediately seaward of the shore, in contrast to the main structure of the shield volcano, dipping more gently (at about 12°) farther away from the shore. This underwater cliff may represent the head of recent lava flows and be comparable in structure to the "palis" of the southern flank of the Big Island. Using simple geometrical optics, and Watts and ten Brink's (1989) crustal model, we trace rays from the hypocenter to the ocean floor and into the water column. Figure 3a shows that a *P* wave leaving the source at an incidence angle of 80° (10° on the horizontal) will intersect the steep element of slope and can penetrate the SOFAR after only one set of bounces between surface and bottom. [The velocity profile of the SOFAR wave guide requires an incidence of less than 12° on the horizontal for the wave to be trapped inside the channel (Ewing and Worzel, 1948).] The travel time of this converted $P \rightarrow T$ phase will account for a residual of −2.56 sec, as opposed to the observed −2.93 sec. Given the general precision of hypocentral locations, this agreement is excellent, and the difference (−0.37 sec), if at all significant, could be easily explained by conversion slightly off the great circle plane. Figure 3b shows that the *S* wave will be very similarly converted with an even better agreement between observed and computed residuals. On the other hand, Figures 3c and 3d show that any conversion of a *P* wave at a point slightly farther away from the shore would take place on a much less steeply dipping ocean floor (typically 12°) and would thus require a more complex series of surface and bottom reverberations before the ray could remain trapped inside the SOFAR channel; this process of "downslope propagation" has been described by Officer (1958) and Johnson *et al.* (1963).

We thus propose that conversion took place at a steep element of ocean floor, documented to be present immediately seaward of the shore of the southern part of the Big Island in the vicinity of 155.12° W (Kaen Point). The simple process of a single reverberation before the ray enters the SOFAR results in an impulsive *T* phase, as recorded 3900 km away and 43 min later in Polynesia. Because successive reflections on the ocean bottom are bound to result in significant amplitude losses, this model, which avoids them, also explains the relatively large amplitudes recorded at PMO. Finally, because of the small extent of the steepest part of the ocean floor, only rays from a limited range of incidence angles at the source (not exceeding 0.6°) will be directly converted into *T* waves, adding to the purity of the signal.

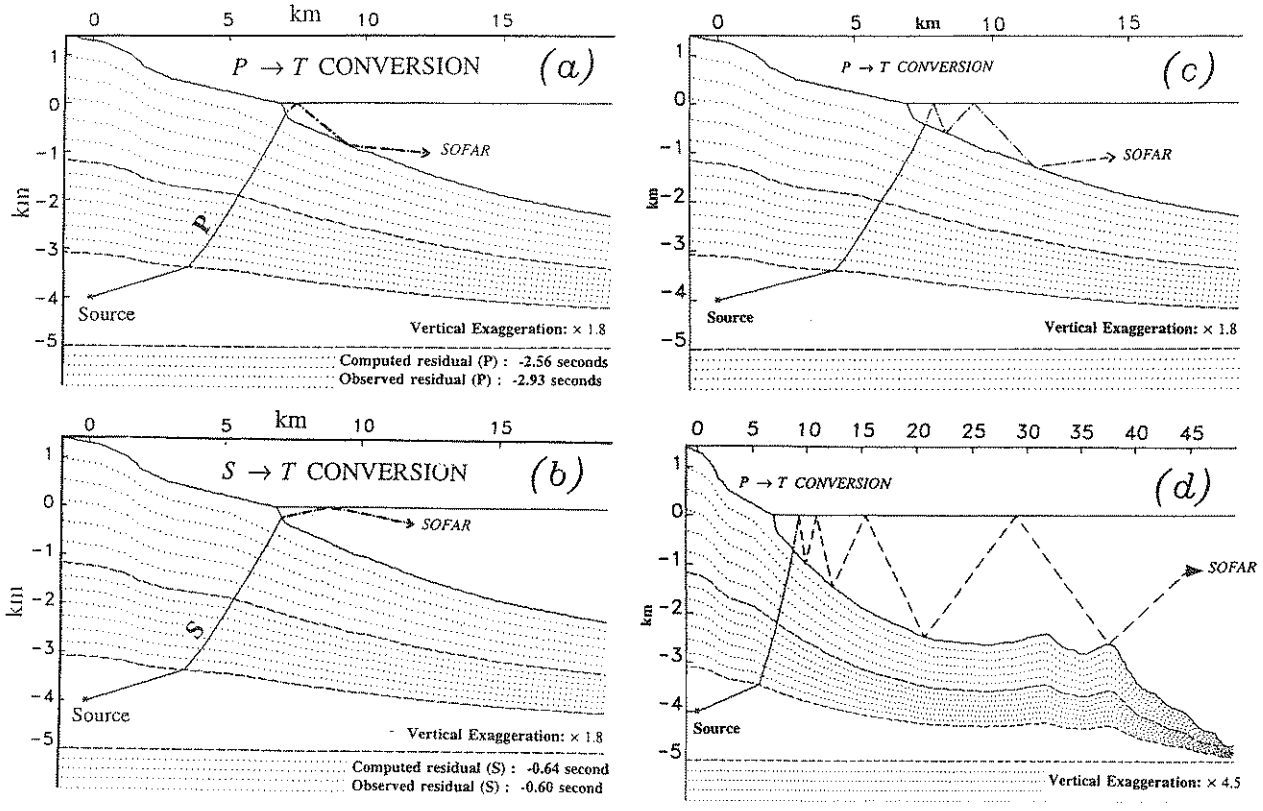

Figure 3. Modeling of the seismic-to-acoustic conversion for the Hawaii earthquake of 8 June 1993. (a) Conversion of a *P*-wave incident upon the steep section of ocean floor. (b) Conversion of an *S*-wave incident upon the steep section of ocean floor. (c) and (d) Case of a *P*-wave incident upon a gently sloping section of ocean floor. The bathymetry in all diagrams is a cross section of Smith's (1994) dataset at the great-circle azimuth (168°) from the epicenter to station PMO. The crustal structure is modeled after Watts and ten Brink (1989); the dotted lines correspond to increments of 0.1 km/sec in the *P* velocity. Note the greater vertical exaggeration in (d).

It is also possible to further explore the question of the spectral content of the two arrivals making up the *T* phase at PMO. Figure 4 compares their Fourier spectra. The first arrival is peaked at $f_P = 7.68$ Hz, whereas the second is peaked at $f_S = 5.05$ Hz. If we focus on those two frequencies, we can quantify this observation through the ratio

$$R_{SP} = \frac{X_P\,(f_S)/X_S\,(f_S)}{X_P\,(f_P)/X_S\,(f_P)} = 0.27 \qquad (2)$$

of the relevant spectral amplitudes *X*. This ratio eliminates unknowns such as focal mechanism geometry and source spectral content and can be taken as representative of the difference in anelastic attenuation for *P* and *S* waves along the seismic path from the source to the conversion point. Assuming further that no bulk attenuation Q_K^{-1} is present, we find that $R_{SP} = 0.27$ leads to a shear attenuation factor $Q_\mu = 21$. This low number is not unreasonable for the volcanic area immediately to the south of Kilauea and is indeed in good agreement with the values inferred by Koyanagi *et*

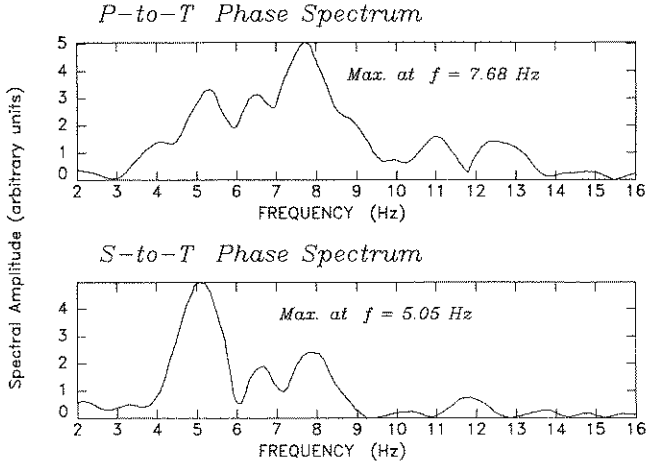

Figure 4. Comparison of the amplitude spectra of the $P \rightarrow T$ and $S \rightarrow T$ phases of the seismogram shown in Figure 2. Each diagram represents the spectrum of a 1-sec window centered on the relevant phase. Vertical scales arbitrary.

al. (1995) ($Q_\mu \approx 30$ in the immediate vicinity of the Kilauea caldera).

Finally, the assumption that the two arrivals making up the *T* phase at PMO correspond to $P \rightarrow T$ and $S \rightarrow T$ conversions at appreciably the same point of the shoreline means that the *T*-phase seismogram at PMO can be regarded as a simple translation in time (by about 2600 sec) of the near-field seismogram at the conversion point. We could not verify this suggestion directly since no seismic station exists at the exact conversion point; furthermore, all stations of the local HVO network went off scale during this $m_b = 5.2$ earthquake. However, we were able to find a record at the nearby station WHA (Wahaula; 19 km from the estimated conversion point) of a small aftershock of the event under study (8 June 1993; 15:38 GMT). We verify in Figure 5 the generally common character of the wave shapes on that record and the *T*-phase record at PMO. Note, however, that the later arrival at WHA, approximately 4 sec after the *S* wave, does not convert into *T* energy, since this presumed surface or interface wave is too low frequency to be trapped inside the SOFAR, its dominant period on the record being 0.5 sec. Slight inconsistencies between *S–P* times on the two records can be attributed to the difference in epicentral distances in the two cases; the aftershock was not located precisely by HVO, and Figure 5 should not be overinterpreted in this respect. The close similarity between the two records confirms the absence of significant dispersion in the relevant range of frequencies for *T* waves propagating in the Pacific over teleseismic distances, an already widely observed property (Cansi, 1981; Okal and Talandier, 1986), which underscores the potential of *T* waves for detection and interpretation of distant marine sources.

Finally, we obtained generally similar results during the recent earthquakes (of smaller magnitude $m_b = 4.2$ and 4.3) on the East Rift of Kilauea on 16 March 1997 and 30 June 1997.

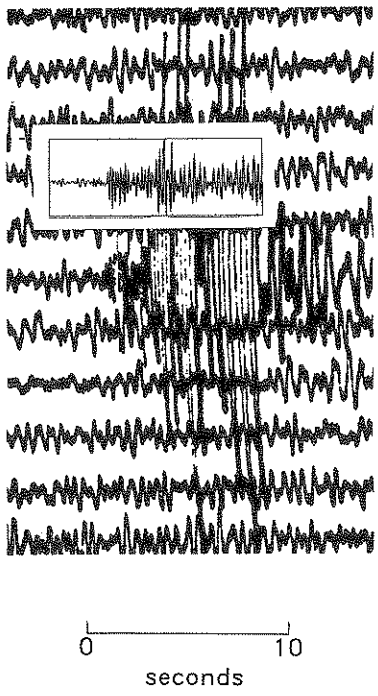

Figure 5. Comparison of seismogram shown in Figure 2 (reproduced at smaller scale; inset) with seismogram of an aftershock of the same event, recorded in the near field at station WHA, 15 km from the source.

The Loihi Earthquake of 29 July 1996

We now turn our attention to the record of the largest earthquake in the Loihi volcanic swarm of the summer of 1996 (29 July 1996; 11:00:32.5 GMT; $m_b = 4.4$). Its location (18.891° N; 155.25° W; $h = 13$ km) and origin time are given in the PDE bulletin, as computed by HVO, but without error bars. The record of its *T* phase at PMO is presented in Figure 6. When comparing this record with Figure 2, a number of differences are immediately apparent. First, the residual is strongly positive (+2.52 sec), suggesting that most of the energy in the *T* wave is delayed in the process of generating the *T* wave (assuming of course a correct combination of hypocenter and origin time). Also, the general character of the arrival is emergent, rather than impulsive, there is no clear separation between $P \rightarrow T$ and $S \rightarrow T$ contributions, and the spectrum of the phase is irregular. Finally, the general level of amplitude recorded (0.8 μm/sec peak-to-peak) is about 20 times less than for the 1993 earthquake.

Since the two epicenters are only 49 km apart and the recording takes place some 3900 km away, the receiver-side geometry is fundamentally equivalent for the two earthquakes, and thus any differences cannot be due to receiver artifacts, but rather express different processes at the seismic-to-acoustic conversion. The characteristics of the Loihi record argue for a complex and relatively inefficient transfer of seismic energy to the water column.

The propagation and conversion of seismic rays from Loihi is investigated in Figure 7. Note that, with a maximum dip of 19°, the slope of the ocean floor at Loihi is more gentle than along the Big Island shore and, in particular, that no steep cliffs are documented in this cross section. As such, the conversion must take place at an unfavorable angle, requiring several episodes of reverberation (with the resulting losses in amplitude) before the ray can remain trapped inside the SOFAR channel. Figure 7 shows that this is the case both for *P* and *S* waves and that for both types of seismic waves, a large range of incidences can funnel their rays into the SOFAR channel. The interference between these various components gives rise to an emergent *T* phase, of relatively low amplitude, and in which the $S \rightarrow T$ component will be mixed with late $P \rightarrow T$ contributions, as indeed observed on the actual record.

While this model explains the general characteristics of the teleseismic *T* phase, the fit between the observed residual (+2.52 sec) and the computed residual for the model in Figure 7 (+4.98 sec) is poor. We believe that this may be

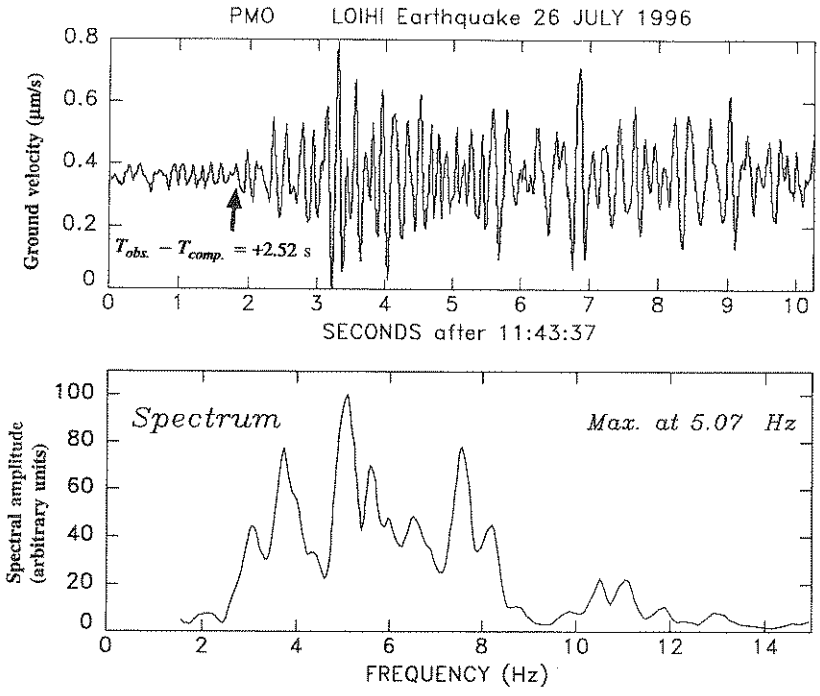

Figure 6. Seismogram (*Top*) and spectrum (*Bottom*) of the *T* phase from the Loihi event recorded at PMO. Note differences as described in text with Figures 2 and 4.

due to the generally low precision of the hypocentral solution reported by the NEIC: A better agreement would be obtained by simply adopting a shallower focus.

In conclusion, this section illustrates the critical importance of steep slope elements for the efficient conversion of seismic energy into acoustic *T* waves. We will see that largely similar results are derived for the converse problem on the receiver side.

Mechanism of the Acoustic-to-Seismic Conversion

In this section, we study the opposite phenomenon, namely, the conversion, at a receiving shore, of *T*-wave energy to seismic waves that can then propagate through the island structure. While the problem would appear to be the mirror image of the seismic-to-acoustic conversion studied earlier, a significant difference arises in that a receiver (seismic station) is always located on the surface of the Earth (occasionally well above sea level), whereas an earthquake source is most often buried at least a few kilometers into the Earth.

Our goal is to understand the conditions under which various kinds of seismic waves (*P, S,* and surface) can be generated. For this purpose, we use marine sources, thus eliminating the additional complexity resulting from the source-side effects described in the previous section. An example of the quality of the records used is given in Figure 8. Specifically, our dataset is comprised of the following:

1. Fourteen marine shots from Operation Midplate (Weigel, 1990), ranging in yield from 25 to 1000 kg and detonated in 1989 in the vicinity of the Society Islands.
2. A series of 13 shots detonated in 1985 off the Coast of Mexico as part of a crustal structure study of the Mexican trench (Nava *et al.,* 1988).
3. A single shot detonated off Vancouver Island on 21 August 1980.
4. Explosive events from the initial phases of volcanic activity at Macdonald Volcano (Talandier and Okal, 1987a).
5. A series of episodes of largely monochromatic *T* waves generated at the Hollister Ridge volcanic source, as described by Talandier and Okal (1996).

For the latter natural events, whose source is uncontrolled both in time and space, we use arrival times at various Polynesian stations, relative to Station VAH (Vaihoa) on the southern coast of Rangiroa Atoll, for which no receiver-side effect is present for *T* waves from the south (see Introduction).

Following the approach in the second section, we define for each record a residual given by equation (1), which again compares the actual travel time of the phase recorded on the seismogram with the expected arrival time, had the whole propagation been oceanic. The residual now arises from the propagation as a (faster) seismic wave over the small portion of the path located in the receiving island structure. This residual is equivalent to a *station correction* that should be applied to the *T*-wave travel-time algorithm in order to properly predict the arrival time of a *T* phase at an island station. However, because Res is expected to be negative (seismic velocities are generally faster than the speed of sound in water), we consider the correction

$$C = -\mathrm{Res} \qquad (3)$$

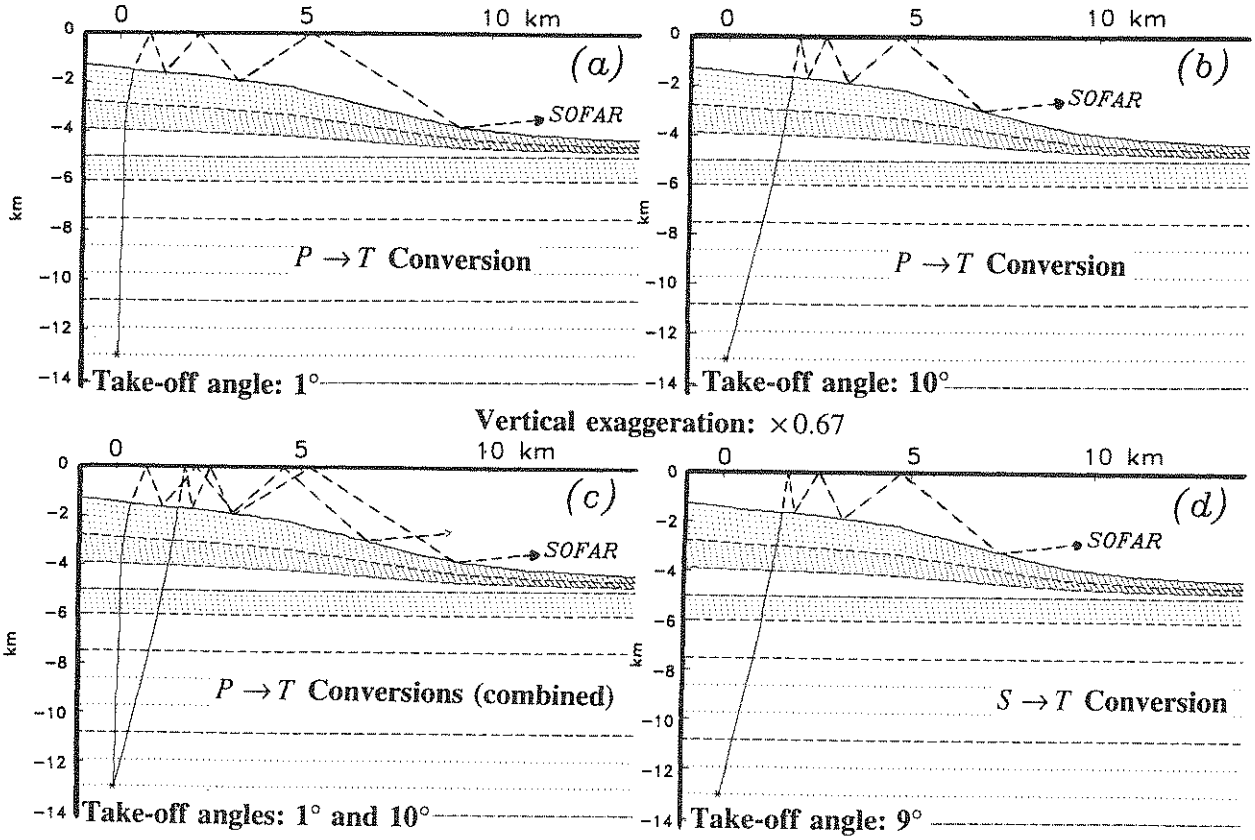

Figure 7. Modeling of the conversion of seismic-to-acoustic energy for the 1996 Loihi earthquake. This figure is similar to Figure 3, but note the absence of steep slopes in the bathymetry. (a) Case of a *P* wave leaving the source at an incidence of 1° from the vertical. (b) Case of a *P* wave leaving the source at 10° incidence. (c) Combination of (a) and (b), illustrating the buildup of a *T* wave as a complex superposition of many rays having undergone relatively inefficient conversions. (d) Case of an *S* wave leaving the source at 9° incidence.

and attempt to model it as a crustal (or conceivably mantle) phase of the island structure. If we make the simplifying assumption of a horizontally layered crustal structure, C is expected to take the form

$$C = \frac{\Delta}{V_T} - \left(\frac{\Delta}{V_i} + K_i\right), \tag{4}$$

where Δ is the horizontal distance traveled inland as a seismic wave, V_T the speed of sound in the SOFAR channel (1484 m/sec), and V_i (velocity) and K_i (zero intercept) are the parameters relative to the ith layer, in which the seismic ray will bottom. V_i could *a priori* be either a P or an S velocity.

In Figure 9, we show the theoretical curves $C = C(\Delta)$ computed using a crustal model adequate for Polynesian shield islands (Talandier and Okal, 1987b) and for land propagation both as a P wave (solid line) and an S wave (dashed line). We also show the values of C expected for land propagation as a guided (surface) wave at a velocity of 2 km/sec (dash-dot line). (Note that the "P times" appear longer than the "S times" simply because these actually represent the *advance* of the wave over a hypothetical T time to the station and incorporate the minus sign in equation 3.)

In a first step, we assume that the acoustic-to-seismic conversion takes place in the vicinity of the underwater cliff of the coral reef and interpret Δ as that section of the great-circle path from source to receiver landward of the conversion point. The resulting data points are plotted as individual symbols in Figure 9 (circles for stations on Tahiti and nearby Moorea; diamonds for station RKT in the Gambier islands). It is immediately apparent that

1. The correlation with P travel times is generally excellent for $\Delta \geqq 9$ km ($C \geqq 4$ sec).
2. In that range of distances ($\Delta \geqq 9$ km), we find no correlation with S times.
3. For $\Delta < 9$ km, the results are imprecise but would suggest conversion to an S wave (or a surface wave); we show these points as half-tone symbols.
4. Four points, shown as open symbols, do not follow the above pattern. Among them, three have exceedingly neg-

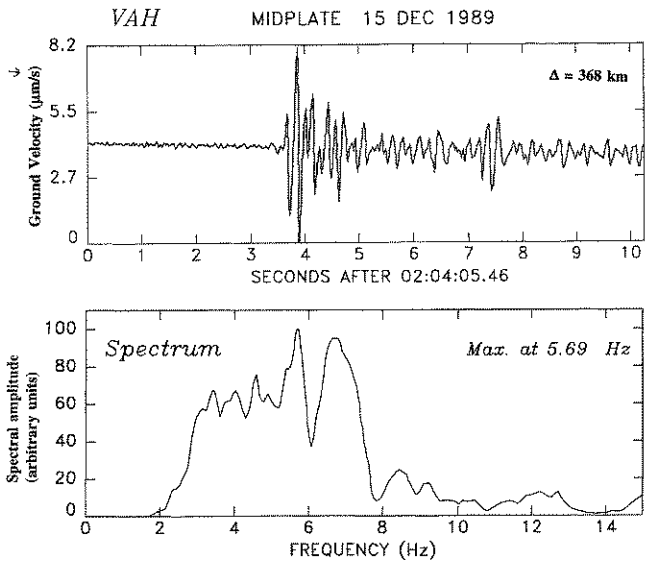

Figure 8. Example of T-phase seismogram, as recorded at VAH for a mid-plate explosion. (*Top*) Time series: note excellent impulsive arrival. (*Bottom*) Spectrum; note breadth between 3 and 7 Hz.

ative residuals; that is, the wave is significantly early at the station: Hollister Ridge to PPN ($C = 19.6$ sec); Macdonald Volcano to PAE ($C = 8.9$ sec), and Midplate to PPT ($C = 6.0$ sec). The fourth, Macdonald to RKT, is if anything slightly late ($C = -0.6$ sec).

An explanation for these outliers is provided in the next paragraphs.

If, in turn, we *assume* that the acoustic-to-seismic conversion generates P waves (at least for times $C \geqq 4$ sec) and invert the observed values of C in equation (3) for Δ, we find that the resulting distances agree spectacularly well with zones of steep cliffs along the coral reefs of the island edifices, as shown in Figure 10. In the case of Tahiti, the three fast times can also be interpreted by solving for Δ (respectively, 40.8, 20.8, and 15.4 km), and noting that, due to the irregular geometry of the island coast, alternate sites can be found on the reef structure at those distances but slightly off the great circle between source and station, at a location where it is inferred that the acoustic-to-seismic conversion must be more favorable. Figure 10 also shows that any attempt to interpret records of T phases on the island of Tahiti as due to $T \rightarrow S$ conversions would require much longer seismic paths, which would move the conversion points far out at sea, where in several instances the bathymetry would actually be deeper than the bottom of the SOFAR channel. In this respect, we can rule out conversion to an S wave for $\Delta \geqq 9$ km.

Figure 9 shows that at distances shorter than about 8 km, the arrival time of a T phase is significantly delayed with respect to the expected $T \rightarrow P$ conversion. The origin of this feature can be explored by studying systematically the conversion of an acoustic ray propagating in the SOFAR channel as it hits the structure of the island of Tahiti, due north of Papeete harbor. For this purpose, we looped over a large number of initial depths (within the SOFAR channel) and grazing angles (within the 12° limit) and evaluated the possibility of generating a P wave in the basaltic shield structure of the island. For the sake of efficiency in the conversion process, we envision only direct conversions and do not consider multiple reverberations. Representative results, shown in Figure 11, indicate that

1. Conversion on the low-dipping interface where the slope is at most 16° is impossible; in such cases, only a surface wave may be recorded, a conclusion upheld by Piserchia *et al.* (1997).
2. Efficient conversion takes place only on the steeply dipping coral reef structure documented in the bathymetry in the immediate vicinity of the island shore (where the slope reaches 55° to 65°). This type of conversion must involve a prior surface reflection of the acoustic ray.
3. The resulting ray for the P wave is steeply inclined downward into the island structure. This property explains that, in order to reach a receiver at the surface, the converted P ray will need to be refracted and thus will be recorded only after some horizontal distance, which will depend on the crustal structure of the island, thereby leading to a kind of "shadow zone" for the $T \rightarrow P$ ray, which we associate with our observation that no P waves are recorded at distances shorter than about 8 to 9 km.
4. Conversion to an S phase is also possible and may result in a ray either more or less steeply dipping than its P analog, depending on the particular incidence of the T wave. In favorable geometries when the $T \rightarrow S$ ray may be less inclined on the horizontal, it will refract at shorter distances and become observable at least over a part of the P shadow. Also, depending on the exact geometry of the refraction, conversion to an S phase may occasionally be possible from a SOFAR ray incident on a less steeply dipping slope than required for $T \rightarrow P$ conversion. In unfavorable geometries, on the other hand, the S wave could be dipping steeper into the solid Earth and could develop a more important shadow zone than the P wave, as suggested by Piserchia *et al.*'s (1997) results for slopes of $\approx 30°$.

These results generally reciprocate our findings relative to the seismic-to-acoustic conversion near the source detailed in the previous section.

Finally, at very short distances, the precision of the measurements is insufficient to distinguish between the various possible conversions, and it becomes futile to interpret the data further; these are the few points plotted as solid circles to the extreme left of Figure 9.

The Particular Case of Station RKT (Rikitea, Gambier). Station RKT, in the Gambier Islands (Figure 12), provides a natural laboratory for examining a large number of possible geometries. The Gambier Islands are generally interpreted

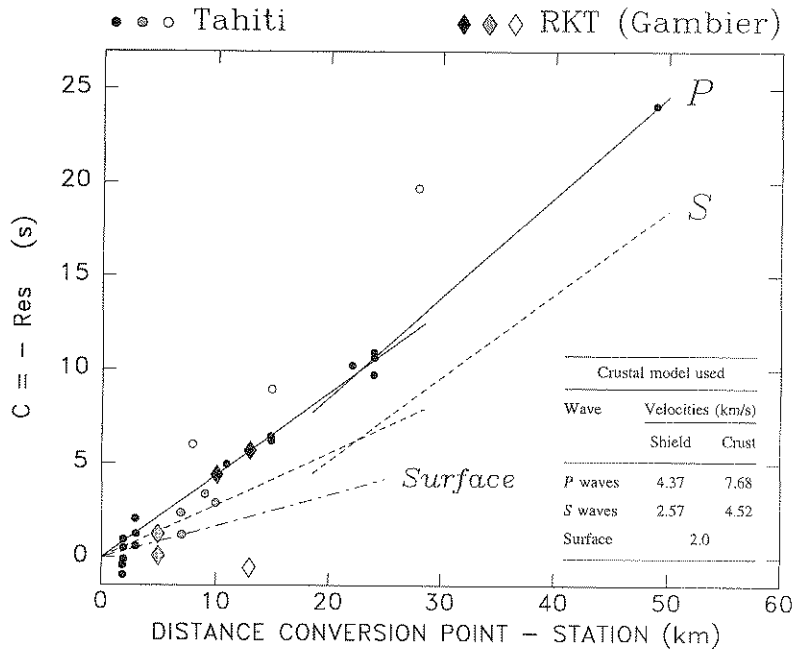

Figure 9. Theoretical value of the opposite, C of the residual (4) plotted as a function of the distance Δ traveled onland, as computed for the crustal model outlined at bottom right. Each symbol represents an observation (circles: Society Islands; diamonds: Rikitea), under the simple assumption of conversion taking place on the receiving shore along the great-circle epicenter station. Note the generally excellent agreement with the curve predicted for a $T \rightarrow P$ conversion (solid symbols). At distances shorter than 9°, conversion to S (or surface) wave seems favored (half-tone symbols). Explanations for the outliers in clear disagreement with those trends are given in the text.

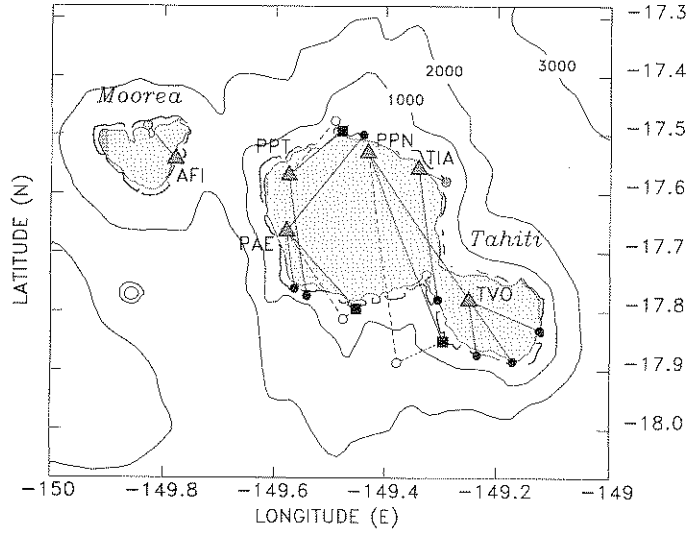

Figure 10. Map of the Islands of Tahiti and Moorea showing short-period stations used in this study (triangles). The coral reef segments around the islands are shown as the fat lines. A representative number of land paths for seismic conversion of T waves are also shown. The solid segments are drawn along the great circle to the source, and their length is inferred from inverting C from equation (4). In agreement with Figure 9, a solid symbol is plotted if $\Delta \geqq 9$ km, a half-tone one otherwise. The three outliers in Figure 9 are shown as open symbols and the relevant paths as dashed lines. Note, however, that in all three cases, nearby alternate conversion points can be found at appropriate distances from the station (shown as full squares).

as the remnants of the 6-million-year-old expression of the Pitcairn hotspot (Brousse *et al.*, 1972). They consist of a diamond-shaped lagoon approximately 20 by 30 km in size. The only exposed volcanic structures are a few islets, among them Mangareva, rising to 441 m altitude, and on which the station RKT is located. Due to asymmetric subsidence, the coral reef is developed only on the northwest, north, and east sides of the atoll, but absent on its southwest and south fringes. This and the geographical location of Mangareva slightly off center of the atoll combine to provide a variety of environments for the acoustic-to-seismic conversion:

- T waves incident from Mexico or Vancouver Island are converted at the northern or northeastern shores of the atoll, in the presence of a well-developed (hence steep) coral reef, and at distances to RKT ranging from 10 to 13 km. Under this geometry, the above model predicts conversion to a P phase refracted into the island and recorded at RKT. These observed phases are plotted as solid diamonds in Figure 9.
- T waves incident from the Midplate experiment are converted at the very end of the well-developed reef, but in all cases, at a distance from RKT of only 6 to 7 km. RKT then sits in the shadow of any possible converted P wave, and only a later arrival (interpreted as a surface wave) is observed. These phases are plotted as half-tone diamonds in Figure 9.
- T waves from the southwest (Macdonald Seamount) or south (Hollister Ridge) are incident at a point where the reef structure is poorly developed or absent. Without a steep cliff, an efficient conversion into a body wave is not

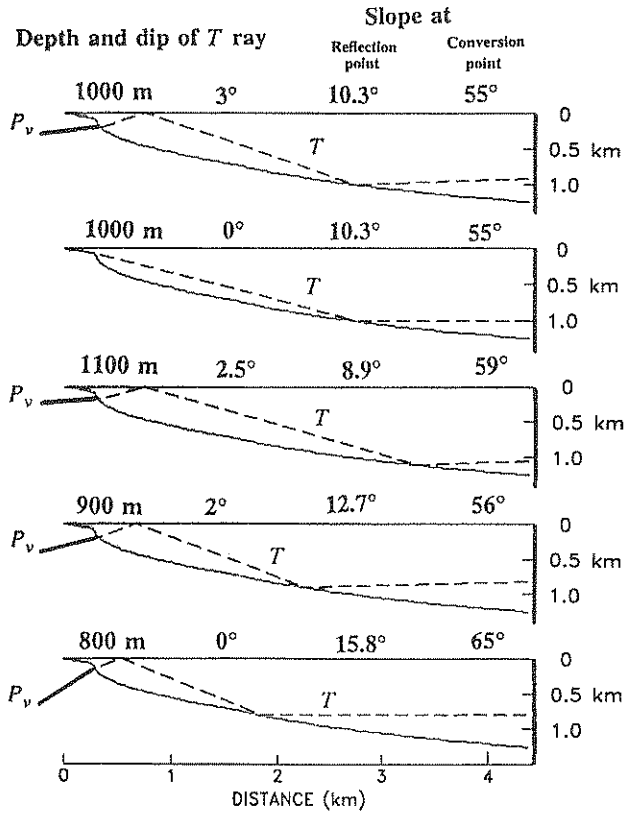

Figure 11. Modeling of the acoustic–seismic conversion seaward of Papeete Harbor, Tahiti. We consider rays at variable depths and inclinations in the SOFAR channel, 4 km seaward of the coral structure, and study their reverberations between surface and bottom. This representative set shows that only those rays reaching the steepest element of shore will penetrate into the island as P waves and that the resulting ray will be inclined downward into the island structure.

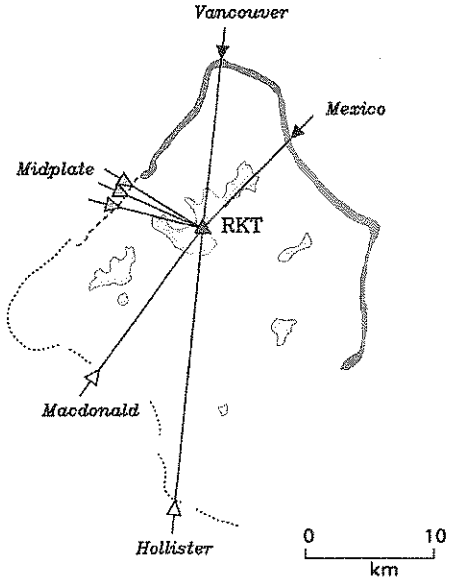

Figure 12. Map of the Gambier Islands showing the directions of arrival at Rikitea (RKT) of the T waves studied in Figure 9. The volcanic islands in the lagoon are shown lightly shaded, while the continuous coral reef to the north and east is shown as dark gray fringe. To the west and south, the coral becomes less developed (shown as dashed and dotted lines). Solid arrows indicate conversion as P wave; half-tone arrows, as S or surface waves; and open arrows indicate propagation in the lagoon as a guided (surface?) wave at very slow speed. See text for details.

possible, and this explains that no $T \rightarrow P$ phase is observed, despite a path inside the atoll as long as 14 km (Macdonald) or even 21 km (Hollister). Rather, we propose that the T-wave energy is converted into a guided wave (a form of Rayleigh, Scholte, or Stoneley wave) at the interface between the water layer and the shallower structures of the edifice. Their dispersion is controlled by the velocity of shear waves in the shallowest, often unconsolidated, detritic, and water-saturated layers of the solid, and this can result in group velocities less than 1 km/sec (Okal and Talandier, 1981; Harkrider and Okal, 1982). This explains the exceedingly slow times observed at RKT for T phases coming from the south (open diamond in Figure 9).

A significant aspect of our results is that, in Polynesia, we fail to observe $T \rightarrow S$ phases as the dominant arrival, except possibly in the small range of distances near the conversion point corresponding to the P shadow. This is in contrast to the study by Koyanagi *et al.* (1995), who interpreted most arrivals on the Big Island of Hawaii from earthquakes in North America as converted $T \rightarrow S$ phases. This inconsistency deserves further discussion.

We note that the phase velocity of the waves observed by Koyanagi *et al.* (1995) is slower than would be expected over the large extent of their array. In the example given in their Figure 5, it is 1.95 km/sec over the 80 km separating stations NAG and KHU, a distance far in excess of the emergence point of mantle-refracted phases in the models of Ellsworth and Koyanagi (1977) and Hill and Zucca (1987), the latter along an experimental profile practically superimposed with the NAG-KHU path. We would suggest that the absolute maximum of energy in the relevant spectrograms corresponds to a (surface?) wave guided through the shallowest layers of the island and that the converted S arrival may be the relative maximum reaching KHU 60 sec into the spectrogram; this time can be reconciled with a conversion at a point 8 km seaward of NAG, and a subsequent propagation to KHU as a mantle phase through the structure proposed by Hill and Zucca (1987), once appropriately scaled for S waves using a Poisson ratio of 0.25. There remains the intriguing observation that converted $T \rightarrow P$ phases are absent from their records.

This can be explained if one notes that the offshore bathymetry along the segment of coastline from Hilo to Cape Kumuhaki, while steep by the standards of volcanic shield structures (20° as opposed to the more usual 12° for the southern coast of the Big Island), may lack the steepest segments (50° to 60°), corresponding either to coral reefs (Tahiti) or the heads of very recent lava beds (Hawaii), and which, we have seen, are crucial to efficient $T \rightarrow P$ or $P \rightarrow T$ conversions. Such a geometry would explain the absence of *P* waves on the records studied by Koyanagi *et al.* (1995).

Conclusions

This study has established the fundamental role played by steep segments of ocean floor in the vicinity of coastlines in controlling both the seismic-to-acoustic and acoustic-to-seismic conversions. We characterize as steep a section of ocean floor with a slope reaching 45° to 60°. These are typical of the outboard cliffs of the coral reefs making up atolls (e.g., Rangiroa) or surrounding mature volcanic islands (e.g., Tahiti and Gambier) but can also be found locally at the head of very young basaltic flows (south coast of the Big Island; Mehetia).

In the absence of a steep slope, acoustic rays trapped in the SOFAR channel (and as such inclined less than 12° on the horizontal) are post-critical for any simple refraction (both *P* and *S*) into the solid Earth. As a result, on the source side a *T* wave can be successfully generated only following a series of reverberations between the surface and floor of the ocean, the dip of the latter ensuring the eventual shallowing of the ray and its penetration of the SOFAR channel. This process is relatively inefficient and leads to emergent *T* phases with low amplitudes, as was observed in the case of the Loihi earthquake. On the receiver side, and keeping in mind that observations can be made only at the Earth's surface, the conversion can result in a surface-type wave, guided through the shallowest layers of the island's structure, and often characterized by poor propagation and strong attenuation.

Note that the absence of a steep slope is generally the rule in most island environments. As such, the great majority of oceanic earthquakes will generate spindle-shaped emergent *T* phases building up their amplitude very slowly. On the receiver side, the majority of land-based seismic stations will record *T* phases poorly, since the seismic surface waves will be strongly attenuated after traveling only a short distance. Also, because of the combination of many rays converting at different locations, both inside and outside the great-circle plane, the *T*-wave envelope will in general develop a characteristic spindle shape (Cansi and Bethoux, 1985).

On the other hand, in the presence of a steep slope, an efficient refraction is possible between a seismic *P* wave and an acoustic wave with a shallow dip on the horizontal, allowing efficient conversion with at most one reverberation in the water column. On the source side, this process results in impulsive *T* phases, which can carry an undisturbed picture of the near-field strong-motion seismogram to teleseismic distances. On the receiver side, the generation of a *P* wave results in the possibility of the *T* phase being recorded at substantial distances from the shore (in practice, limited only by the size of the receiving island). However, because the *P* wave is refracted downward into the structure and stations are by necessity above sea level, there develops a shadow zone hampering the observation of *P* waves at close distances from the shore.

While the conversion to and from *S* waves generally follows the same principles, the reduced velocity contrast with *T* waves results in lower limits (≈25°) for the steepness of the slope allowing efficient conversion. Similarly, the extent of the shadow zone upon reception on a steep slope may differ from that for *P* conversions, meaning that at distances of 5 to 8 km, *T* waves incident on steep slopes may occasionally be observed as *S* conversions and thus arrive slightly later than would be expected for a *P* conversion.

A final conclusion of this study is that the conversion of *T* phases at island shores and their subsequent propagation overland as seismic phases can be adequately modeled through a residual (Res) that is in the nature of a station correction, thus allowing the precise use of *T* phases for the detection and precise location of small sources at large teleseismic distances in the marine environment.

Acknowledgments

We are grateful to Terri Duennebier for providing an on-line version of Smith's (1994) bathymetry of the southern shore of the Big Island and to Paul Okubo and colleagues for access to the archives at Hawaii Volcano Observatory. Keith McLaughlin provided a careful review of the earlier version of this article.

References

Anonymous (1930). *The Volcano Lett.* **268,** 1–4. Hawaiian Volcano Observatory.

Brousse, R., J.-C. Philippet, G. Guille, and H. Bellon (1972). Géochronométrie des Iles Gambier (Océan Pacifique), *C. R. Acad. Sci. Paris* **274D,** 1995–1998.

Cansi, Y. (1981). Etudes expérimentales d'ondes *T, Thèse de 3ème Cycle,* Orsay, 101 pp.

Cansi, Y. and N. Bethoux (1985). *T* waves with long inland paths: synthetic seismograms, *J. Geophys. Res.* **90,** 5459–5465.

Ellsworth, W. L. and R. Y. Koyanagi (1977). Three-dimensional crust and mantle structure of Kilauea Volcano, Hawaii, *J. Geophys. Res.* **82,** 5379–5394.

Ewing, M. and J. L. Worzel (1948). Long-range sound transmission, *Geol. Soc. Am. Mem.* **27,** 35 pp.

Harkrider, D. G. and E. A. Okal (1982). Propagation and generation of high-frequency sediment-controlled. Rayleigh modes following shallow earthquakes in the southcentral Pacific (abstract), *EOS* **63,** 1025.

Hill, D. P. and J. J. Zucca (1987). Geophysical constraints on the structure of Kilauea and Mauna Loa volcanoes and some implications for seismomagmatic processes, *U.S. Geol. Surv. Profess. Pap.* **1350,** 903–917.

Johnson, R. H., J. Northrop, and R. Eppley (1963). Sources of Pacific *T* phases, *J. Geophys. Res.* **68,** 4251–4260.

Koyanagi, S., K. Aki, N. Biswas, and K. Mayeda (1995). Inferred attenuation from site effect-corrected *T* phases recorded on the Island of Hawaii, *Pure Appl. Geophys.* **144,** 1–17.

Levitus, S., T. P. Boyer, J. Antonov, R. Burgett, and M. E. Conkright (1994). *World Ocean Atlas 1994,* NOAA/NESDIS, Silver Spring, Maryland.

Linehan, J. (1940). Earthquakes in the West Indian region, *Trans. Am. Geophys. Un.* **21,** 229–232.

McLaughlin (1997). *T*-phase observations at San Nicolas Island, California (abstract), *Seism. Res. Lett.* **68,** 296.

Nava, F. A., F. Núñez-Cornú, D. Córdoba, M. Mena, J. Ansorge, M. Rodriguez, E. Banda, S. Müller, A. Udias, M. Garcia-Garcia, G. Calderón, and the Mexican Working Group for Deep Seismic Profiling (1988). Structure of the Middle America trench in Oaxaca, Mexico, *Tectonophysics* **154,** 241–251.

Officer, C. B. (1958). *Introduction to the Theory of Sound Transmission with Its Application to the Ocean,* McGraw-Hill, New York.

Okal, E. A. and J. Talandier (1981). Dispersion of one-second Rayleigh modes through oceanic sediments following shallow earthquakes in the Southcentral Pacific Ocean basin, in *Bottom-Interacting Ocean Acoustics,* W. A. Kuperman and F. B. Jensen (Editors), NATO Confer. Ser., IV:5, 345–358, Plenum, New York.

Okal, E. A. and J. Talandier (1986). *T*-wave duration, magnitudes and seismic moment of an earthquake; application to tsunami warning, *J. Phys. Earth* **34,** 19–42.

Okal, E. A. and J. Talandier (1997). *T* waves from the great 1994 Bolivian deep earthquake in relation to channeling of *S* wave energy up the slab, *J. Geophys. Res.* **102,** 27421–27437.

Okal, E. A., J. Talandier, K. A. Sverdrup, and T. H. Jordan (1980). Seismicity and tectonic stress in the southcentral Pacific, *J. Geophys. Res.* **85,** 6479–6495.

Piserchia, P.-F. J. Virieux, D. Rodrigues, S. Gaffet, and J. Talandier (1997). A hybrid numerical modeling of *T*-wave propagation application the Midplate experiment, *Geophys. J. Int.,* submitted.

Ravet, J. (1940). Remarques sur quelques enregistrements d'ondes à très courte période au cours de tremblements de terre lointains à l'Observatoire du Faiere, Papeete, Tahiti, *Sixth Pacific Sci. Congress,* Vol. 1, pp. 127–130.

Smith, J. R. (1994). Island of Hawaii and Loihi submarine volcano, high-resolution multibeam bathymetry around the Island of Hawaii [1:75,000, 1:250,000, 1:500,000], Sheet 6, Hawaii Seafloor Atlas, Hawaii Institute of Geophysics and Planetology, Honolulu.

Talandier, J. (1993). French Polynesia Tsunami Warning Center (CPPT), *Natural Hazards* **7,** 237–256.

Talandier, J. and G. T. Kuster (1976). Seismicity and submarine volcanic activity in French Polynesia, *J. Geophys. Res.* **81,** 936–948.

Talandier, J. and E. A. Okal (1979). Human perception of *T* waves: the June 22, 1977 Tonga earthquake felt on Tahiti, *Bull. Seism. Soc. Am.* **69,** 1475–1486.

Talandier, J. and E. A. Okal (1987a). Seismic detection of underwater volcanism: the example of French Polynesia, *Pure Appl. Geophys.* **125,** 919–950.

Talandier, J. and E. A. Okal (1987b). Crustal structure in the Tuamotu and Society Islands, French Polynesia, *Geophys. J. R. Astr. Soc.* **88,** 499–528.

Talandier, J. and E. A. Okal (1996). Monochromatic *T* waves from underwater volcanoes in the Pacific Ocean: ringing witnesses to geyser processes? *Bull. Seism. Soc. Am.* **86,** 1529–1544.

Watts, A. B. and U. S. ten Brink (1989). Crustal structure flexure, and subsidence history of the Hawaiian Islands, *J. Geophys. Res.* **94,** 10473–10500.

Weigel, W. (1990). Bericht über die SONNE-Expedition SO65-2, Papeete-Papeete, 7.-28. Dez. 1989, Universität Hamburg, Institut für Geophysik.

Laboratoire de Géophysique
Commissariat à l'Energie Atomique
91680 Bruyères-le-Châtel, France
(J.T.)

Department of Geological Sciences
Northwestern University
Evanston, Illinois, 60208
(E.A.O.)

Manuscript received 27 May 1997.